Inductive Power Transfer System With Constant Current-Constant Voltage Charging Tolerating Misalignment Based on Multiobjective Optimization for Compensation Topology

Qi Wang, Zheng Li, Bin Yang, *Member, IEEE*, Yuanfang Lu, Ruikun Mai, *Senior Member, IEEE*, Zhengyou He, *Senior Member, IEEE*, and Yang Chen, *Senior Member, IEEE*

***Abstract*—Constant current (CC) and constant voltage (CV) outputs are important in the inductive power transfer (IPT) system for battery charging. However, the coupling changes caused by the misalignment between the primary and secondary coils significantly affect the system performance. To address this issue, this article proposes a parameter design method based on the nondominated sorting genetic algorithm-II algorithm for the IPT system to tolerate mutual inductance and load variations in both CC and CV modes. First, a mathematical model of the compensation topology has been established to describe the output characteristics. In addition, the design steps are given to obtain system parameters, and a specific example is designed accordingly. Finally, an experimental setup was built, and the results show that the fluctuation of the output current is less than 0.34% when the load changes from 21 Ω to 24 Ω and the fluctuation of the output voltage is less than 2.69% when the load changes from 24 Ω to 240 Ω as the mutual inductance varies from 20 μH to 30 μH. During the whole process of the CC-CV charging, the maximum efficiency is 93.5%.**

***Index Terms*—Algorithm, constant current (CC), constant voltage (CV), inductive power transfer (IPT), misalignment tolerance.**

I. Introduction

INDUCTIVE power transfer (IPT) system is based on magnetic coupling to transfer energy from a power source to an electrical device without any physical contact. Compared with traditional plug-in power supply, the IPT system is more convenient, user-friendliness, flexible, and safer. Due to these advantages, it has been widely applied to a variety of applications, such as implantable medical devices, portable devices, autonomous underwater vehicles, and electric vehicles [1], [2], [3], [4].

When taking IPT technology for charging, a two-stage charging mode of constant current (CC) and constant voltage (CV) is usually used to extend the battery life and ensure its safety. In the initial stage, the battery is charged in CC mode, and the battery voltage gradually increases. When the voltage reaches a certain value, the charging process is turned into CV mode. The battery current gradually decreases until it is less than a certain value, and the charging ends [5]. Throughout the entire charging process, the equivalent load of the battery is constantly changing, ranging from tens to hundreds of ohms [6]. Besides, for an IPT system, the primary winding connected to the power supply is usually fixed, while the secondary winding is configured on the electric equipment. As a result, it is hard to avoid the misalignment between the pads, which makes misalignment tolerance also a common problem encountered during IPT CC-CV charging. It can lead to a decrease in transmission power, transmission efficiency, and system stability. Therefore, the IPT system is always adopted to realize CC and CV outputs with misalignment tolerance.

To address the above issues, control schemes are straightforward methods for IPT systems to achieve stable output against load and coupling variations. For example, adding a variable inductor [7], variable capacitor [8], or dc–dc converter [9] on the primary or the secondary side can regulate the output. These methods often require the accuracy and speed of the controller based on primary and secondary communication [10]. In addition, if the ranges of load and mutual inductance largely change simultaneously, it can increase the range of modulation depth, which may lead to a decrease in efficiency [11]. As we know, the control method is active regulation, and passive regulation optimizing the compensation topology/pad of the IPT system can also resist the load or coupling variation, which can simplify control schemes [12], [13].

Manuscript received 9 April 2024; revised 21 June 2024; accepted 13 July 2024. Date of publication 30 July 2024; date of current version 26 December 2024. This work was supported in part by the National Natural Science Foundation of China under Grant 52207226, in part by the Sichuan Science and Technology Program under Grant 2023NSFSC0819 and Grant 2023JDRC0102, in part by the Fundamental Research Funds for the Central Universities under Grant 2682024CX025, and in part by the National Key Research and Development Program of China under Grant 2023YFB4302002. Recommended for publication by Associate Editor J. Acero. *(Corresponding author: Yang Chen.)*

Qi Wang, Zheng Li, Bin Yang, Ruikun Mai, Zhengyou He, and Yang Chen are with the School of Electrical Engineering, Southwest Jiaotong University, Sichuan 611756, China (e-mail: wangqi2022@my.swjtu.edu.cn; li_zheng@my.swjtu.edu.cn; yb@my.swjtu.edu.cn; mairk@swjtu.edu.cn; hezy@home.swjtu.edu.cn; yangchen@swjtu.edu.cn).

Yuanfang Lu is with the State Key Laboratory of Alternate Electrical Power System With Renewable Energy Sources, North China Electric Power University, Beijing 102206, China (e-mail: luyuanfang@ncepu.edu.cn).

Color versions of one or more figures in this article are available at https://doi.org/10.1109/TPEL.2024.3435424.

Digital Object Identifier 10.1109/TPEL.2024.3435424

The compensation topology with specialized design is commonly adopted to achieve CC and CV outputs. These methods can be roughly divided into two categories according to whether they can be switched adaptively or not. Incorporate switches on the primary [5], [14], or secondary side [15] to form a switching topology, and the different topology characteristics give convenience to switch from CC to CV mode. However, switching needs to detect the charging voltage and current. To deal with this issue, some scholars have proposed new circuits to realize self-sustain in CC and CV modes. Realizing automatic switching usually requires an auxiliary coil. For example, a three-coil system is used to form a clamp circuit [16], [17]. Based on this, a family of circuit structures with different secondary sides is analyzed [18], and cope with the desired charging profile to configure the output thresholds of the charger with the proper compensation. Even though these methods achieve good implementation of CC and CV, the charge current and voltage of these methods are dramatically affected without the alignment of pads.

Misalignment of the pads usually causes a drop in mutual inductance, which affects the stability of the output. Magnetic coupler design [19], [20], [21], [22], [23], hybrid topology [24], [25], [26], and parameter optimization [27], [28], [29] have been taken to mitigate the problem. Some polarized coil structures like double-D pads [19] and bipolar pads [20] are advocated to build a uniform magnetic field so that coupling variations during offsets are minimized. Asymmetric coils [21] are also used to improve the lateral tolerance of the system. Moreover, antiparallel windings [22] are employed to smooth the coupling coefficient variation over different positions. To exploit the magnetic field generated by both the receiving coil and transmitting coil, a magnetic integration [23] with a shared ferrite layer is designed to achieve CC output. More coils to cooperate with the design are needed to enhance the system performance of misalignment tolerance, which is more complex. Concerning the hybrid topology structure, it is often combined with two topologies, and the output gain of the two topologies is opposite to the change in mutual inductance. By designing reasonable parameters, the total output gain of the system is relatively constant within a certain offset range. For example, it can be a combination of inductor-capacitor-capacitor-series (LCC-S) and S-LCC topologies with input-parallel/series-output-series/parallel structure [24], or inductor-capacitor-inductor-inductor-capacitor-capacitor (LCL-LCC) and series–series (SS) topologies with input-parallel/series-output-parallel/series structure [25]. Besides, four-coil couplers can also tolerate misalignment [10], [26]. Hybrid topologies are more complex with more components. To simplify the coil design and complexity, parameter design is commonly adopted. In [27] and [11], two design parameter methods are proposed for SS and LCL-S topologies, which can make the maximum power drop no more than 20% when the coupling coefficient changes from 0.08 to 0.2. However, they are limited by the fixed value of load. To address this issue, a family of compensation topologies is used to design compensation parameters with strong misalignment tolerance [28]. With the resistance load varying three times and coupling coefficient varying from 0.21 to 0.35, CC output with 5.78% fluctuation and CV output with 5.57% fluctuation can be achieved, respectively. Moreover, The S-CLC [29] topologies can be combined with particle swarm optimization to increase the range of load variation. When the coupling coefficient increases from 0.2 to 0.4 while the load increases from 50 Ω to 100 Ω, the output voltage ripple is less than 6.61%. However, the abovementioned methods usually only achieve CC, CV, constant power output, or even neither of them, missing the CC-CV charging function.

To resist a certain coupling coefficient range and achieve CC and CV outputs simultaneously, there are mainly three approaches. The first one is the combination of magnetic coupler design (two coils connected reversely in series are applied on the primary side) and automatic switching topology (SS and S/LCC topologies) [30]. It can make the output fluctuations in CC and CV modes less than 5% when the load varies ten times and 250 mm, 30 mm, or 15 mm misalignment in the *X*-, *Y*-, or *Z*-axis, respectively. The second one is a magnetic coupler design with a switching topology. For example, a three-coil hybrid IPT system adds two mode switches that can satisfy CC and CV outputs with improved tolerance of coupling variation and load-independent output [31]. The last one is the hybrid topology connecting with switching topology [32], [33], [34], such as a series of hybrid topologies based on T-type and S-type networks [32] and a hybrid topology formed by LCC-S and S-LCC topologies [33]. Furthermore, an LCC-S series hybrid topology with the configurable topology [34] performs the same function. The fluctuations in CC and CV mode less than 5% can be achieved when the range of coupling coefficient is 0.1 to 0.2 and the loads vary from 19 Ω to 70 Ω. Since the hybrid topology with three or four magnetic couplers has a larger number of components, the complexity of parameter design, system quality, and high cost are nearly inevitable.

The main contributions of this article are as follows.

1) An optimal method of the compensation parameters based on ST-type topology is proposed. The CC-CV charging can be achieved considering the variations of the coupling coefficient and load simultaneously. The proposed method has fewer components without wireless communication, dedicated coil design, or complicated control compared to the prior related works.
2) The system with the optimized parameters can realize multiobjectives under multiple limitations: output current and voltage fluctuations, total losses, and ZVS condition. The nondominated sorting genetic algorithm-II (NSGA-II) [35], which has the advantages of easy implementation, fast convergence speed, and high accuracy, is adopted to obtain the parameters.

The rest of this article is expressed as follows. Section II analyzes the basic structure and output characteristics of the compensation topologies. An introduction to the NSGA-II algorithm and the unified mathematical model of the system parameters based on this algorithm is given in Section III. In Section IV, the feasibility of the parameters designed by the algorithm is verified. Finally, Section V concludes this article.

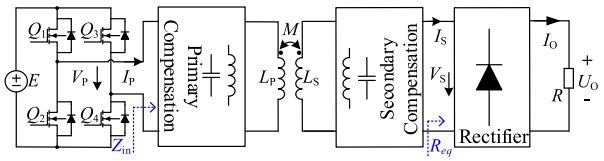

Fig. 1. Equivalent two-port network of the IPT system.

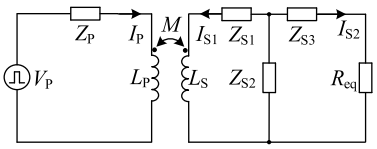

Fig. 2. ST-type compensation topology of IPT system.

II. System Topology Analysis

To simplify the analysis, the IPT system is equivalent to three cascaded two-part networks, which are the primary-side compensated topology, the magnetic coupler network, and the secondary-side compensated topology, as shown in Fig. 1. The two-port network is driven by an inverter with angular frequency $\omega = 2\pi f$, where f represents the switching frequency of the inverter. The input dc voltage E is converted by the full-bridge inverter (Q_1–Q_4) to a high-frequency ac voltage V_P. U_O, I_O, and R_{eq} are the output voltage of the load-side output voltage, the load-side output current, and the equivalent ac load, respectively. It can be expressed in

$$V_P = \frac{2\sqrt{2}}{\pi}E,\quad R_{eq} = \frac{8}{\pi^2}R,\quad U_O = \frac{\pi}{2\sqrt{2}}V_S,\quad I_O = \frac{2\sqrt{2}}{\pi}I_S \tag{1}$$

To reduce the number of the system's components and increase the design flexibility, the ST-type compensation topology, as shown in Fig. 2, is used to design the CC-CV charging IPT system. I_P and I_{S1} are the currents of the primary and secondary coils, respectively. I_{S2} is the input current of the rectifier.

According to Kirchhoff's voltage law, the mathematical model of the ST-type compensation topology of the IPT system can be expressed as follows:

$$\begin{cases} I_P(Z_P + j\omega L_P) + j\omega M I_{S1} = V_P \\ I_{S1}(Z_{S1} + Z_{S2} + j\omega L_S) + j\omega M I_P + Z_{S2} I_{S2} = 0 \\ I_{S2}(Z_{S2} + Z_{S3} + R_{eq}) + Z_{S2} I_{S1} = 0 \end{cases} \tag{2}$$

Associating (1) and (3), the output voltage U_O, output current I_O, and input impedance Z_{in} are solved as

$$\begin{cases} U_O = \dfrac{2\sqrt{2}MZ_{s3}}{\frac{8AR}{\pi} + j\omega\pi^2\left(A(Z_{s2}+Z_{s3}) - {Z_{s3}}^2(L_p+Z_p)\right)}E \\ I_O = \dfrac{8MZ_{s3}}{8AR + j\omega\pi^2\left(A(Z_{s2}+Z_{s3}) - {Z_{s3}}^2(L_p+Z_p)\right)}E \\ Z_{in} = \dfrac{\omega((M^2 - \omega L_p L_s)B + L_p C)}{C + j\omega L_s B} \end{cases} \tag{3}$$

where

$$A = -M^2 + (L_p + Z_p)(Z_{s1} + Z_{s2} + L_s)$$
$$B = 8R + \pi^2(Z_{s2} + Z_{s3})$$
$$C = \left(8R + \pi^2 Z_{s3}\right)(Z_{s1} + Z_{s2}).$$

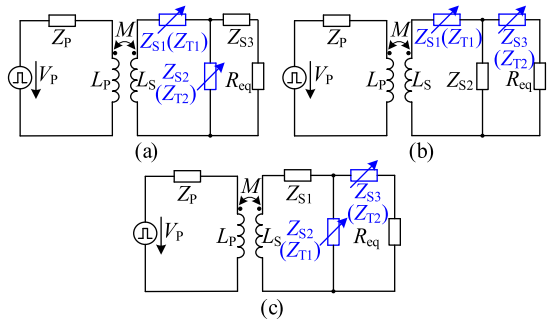

Fig. 3. ST-type compensation topology with two variable parameters.

From (3), coupling-independent outputs cannot be achieved in the system. Coil misalignment can easily damage CC and CV outputs, and compensation component parameters can also affect the value of U_O and I_O. To make the IPT system have the inherent characteristics of tolerating the misalignment and stabilizing output current and voltage, the parameters of the IPT system must be properly designed.

III. Parameter Design and Optimization

For the ST-type compensation topology of the IPT system, it should achieve the following requirements.

1) CC-CV charging function.
2) Tolerating certain ranges of coupling and load.
3) Low fluctuation in CC or CV mode.
4) No communication between the primary and secondary sides.
5) As few components as possible.

Considering the multiple objectives, it is difficult to satisfy all of them when there is only one component as a variable [29]. Therefore, two components on the secondary side are preferred to be chosen as variables, which have three cases, as shown in Fig. 3. In each case, Z_{T1} and Z_{T2} denote the values of the two variables when the system is switched from CC mode to CV mode, respectively.

A. Introduction to NSGA- II Based on Nondominated Sorting

The NSGA-II is different from the single-objective particle swarm optimization algorithm. It is based on nondominated sorting and can set multiple objectives for the system by not designing additional weights. The NSGA-II based on nondominated sorting can be used to better design the IPT system with misalignment tolerance and CC or CV output.

As shown in Fig. 4, taking the minimization of multiobjective optimization problem as an example. For N objective functions $f_i(x)$, $i = 1, 2, \ldots, N$, the set of solutions that " reduce the value of other objective functions without increasing the value of one objective function" is called the Pareto Front.

B. Defining the Decision Variables and Subspace

The choice of decision variables with the subspaces is the primary issue in the parameter design of the compensation

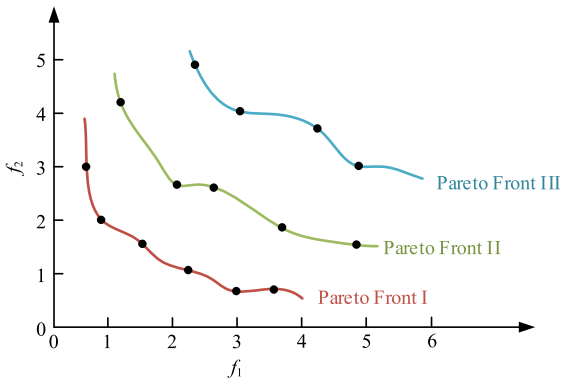

Fig. 4. Pareto rating diagram.

topology. For the ST topology, its compensation parameters Z_{P}, Z_{S1}, Z_{S2}, Z_{S3}, and the to-be-switched parameters Z_{T1} and Z_{T2} are used as a part of the decision variables. Besides, E is also used as a decision variable to make the IPT system work within the required input range. As a result, the design of compensation topology for the CC-CV charging with antimisalignment is treated as a seven-dimensional optimization problem.

For the compensation parameters Z_{P}, Z_{S1}, Z_{S2}, Z_{S3}, and the parameters to be switched Z_{T1} and Z_{T2}. The subspaces are limited by the values of the passive compensation parameters, which are limited by their cost, size, and tolerance. Therefore, the limitations of the values of the compensation parameters are given as

$$Z \in [Z_{\min}, Z_{\max}] \tag{4}$$

For the input voltage E, the value should be within a reasonable range, which is given as follows:

$$E \in [E_{\min}, E_{\max}] \tag{5}$$

C. Defining the Objective Function

1) Objective Functions for CC and CV Outputs: The output fluctuation of the IPT system is the main concern when considering the variation of the coupling coefficient. The optimization objective of its output current or output voltage fluctuation can be defined as the integral of the output fluctuations within the operating range of the IPT system, as shown in

$$\begin{aligned} &f_{\mathrm{I}}\left(Z_{\mathrm{P}}, Z_{\mathrm{S1}}, Z_{\mathrm{S2}}, Z_{\mathrm{S3}}, Z_{\mathrm{T1}}, Z_{\mathrm{T2}}, E\right) \\ &\quad = \int_{M_{\min}}^{M_{\max}} \int_{R_{\mathrm{CC\_min}}}^{R_{\mathrm{CC\_max}}} |I_{\mathrm{o}} - I_{\mathrm{N}}| dR dM \end{aligned} \tag{6}$$

$$\begin{aligned} &f_{\mathrm{U}}\left(Z_{\mathrm{P}}, Z_{\mathrm{S1}}, Z_{\mathrm{S2}}, Z_{\mathrm{S3}}, Z_{\mathrm{T1}}, Z_{\mathrm{T2}}, E\right) \\ &\quad = \int_{M_{\min}}^{M_{\max}} \int_{R_{\mathrm{CV\_min}}}^{R_{\mathrm{CV\_max}}} |U_{\mathrm{o}} - U_{\mathrm{N}}| dR dM \end{aligned} \tag{7}$$

where I_{N} and U_{N} are the rated output current and rated output voltage, respectively. The range of the mutual inductance is $[M_{\min}, M_{\max}]$. The range of resistance in CC and CV modes are $[R_{\mathrm{CC\_min}}, R_{\mathrm{CC\_max}}]$ and $[R_{\mathrm{CV\_min}}, R_{\mathrm{CV\_max}}]$, respectively.

2) Objective Functions and Constraints for Efficiency: The IPT system may operate in a detuned state with variations of coupling coefficient and load, which increases the losses of the inverter, coils, and rectifier.

The inverter power loss P_{Inverter} consists of MOSFET turn-ON loss $P_{\mathrm{SW\_ON}}$, conduction loss P_{Cond}, and turn-OFF loss $P_{\mathrm{SW\_OFF}}$. For the turn-ON loss $P_{\mathrm{SW\_ON}}$, zero voltage switching (ZVS) of the MOSFET can reduce or even eliminate the turn-ON loss of the MOSFET. Therefore, the compensation topology parameters should make the input impedance of the system inductive over the operating range of the system, which can reduce the inverter power loss

$$\begin{aligned} &\angle Z_{\mathrm{in}}(M, R_1) > 0, \quad \angle Z_{\mathrm{in}}(M, R_2) > 0 \\ &M \in [M_{\min}, M_{\max}], R_1 \in [R_{\mathrm{CC\_min}}, R_{\mathrm{CC\_max}}] \\ &R_2 \in [R_{\mathrm{CV\_min}}, R_{\mathrm{CV\_max}}] \end{aligned} \tag{8}$$

It should be noted that if the system input impedance is too inductive, although ZVS can be realized, too large input current will also cause the MOSFET to generate additional conduction loss and turn-OFF loss. For the conduction loss P_{Cond} and turn-OFF loss $P_{\mathrm{SW\_OFF}}$, it can be expressed as [37]

$$\begin{aligned} &P_{\mathrm{Cond}}(M, R_1) + P_{\mathrm{SW\_off}}(M, R_1) = 2I_{\mathrm{P}}(M, R_1)^2 r_{\mathrm{m}} \\ &\quad + 4\sqrt{2}E\left|I_{\mathrm{P}}(M, R_1)\right| \left|\sin\left[\angle Z_{\mathrm{in}}(M, R_1)\right]\right| \\ &\quad \times \left(\frac{E_{\mathrm{off}}}{V_{\mathrm{DD}} I_{\mathrm{D}}} + \frac{Q_{\mathrm{RR}}}{I_{\mathrm{R\_D}}}\right) f \\ &P_{\mathrm{Cond}}(M, R_2) + P_{\mathrm{SW\_off}}(M, R_2) = 2I_{\mathrm{P}}(M, R_2)^2 r_{\mathrm{m}} \\ &\quad + 4\sqrt{2}E\left|I_{\mathrm{P}}(M, R_2)\right| \left|\sin\left[\angle Z_{\mathrm{in}}(M, R_2)\right]\right| \\ &\quad \times \left(\frac{E_{\mathrm{off}}}{V_{\mathrm{DD}} I_{\mathrm{D}}} + \frac{Q_{\mathrm{RR}}}{I_{\mathrm{R\_D}}}\right) f \end{aligned} \tag{9}$$

where r_{m} is the forward conduction resistance of the MOSFET; E_{OFF} is the MOSFET turn-OFF loss measured under the test condition "MOSFET voltage at both ends is V_{DD} turn-OFF current is I_{D}". Q_{RR} is the reverse recovery charge of the diode. $I_{\mathrm{R\text{-}D}}$ is the reverse recovery current of the diode, and the above parameters can be obtained from the datasheet provided by the device manufacturer. The above parameters can be obtained from the datasheet provided by the device manufacturer.

The coil loss of the IPT system can be obtained as

$$\begin{aligned} &P_{\mathrm{Coils}}(M, R_1) = P_{\mathrm{Coils\_P}}(M, R_1) + P_{\mathrm{Coils\_S}}(M, R_1) \\ &\quad = I_{\mathrm{P}}(M, R_1)^2 r_{\mathrm{P}} + I_{\mathrm{S}}(M, R_1)^2 r_S \\ &P_{\mathrm{Coils}}(M, R_2) = P_{\mathrm{Coils\_P}}(M, R_2) + P_{\mathrm{Coils\_S}}(M, R_2) \\ &\quad = I_{\mathrm{P}}(M, R_2)^2 r_{\mathrm{P}} + I_{\mathrm{S}}(M, R_2)^2 r_S \\ &M \in [M_{\min}, M_{\max}], R_1 \in [R_{\mathrm{CC\_min}}, R_{\mathrm{CC\_max}}] \\ &R_2 \in [R_{\mathrm{CV\_min}}, R_{\mathrm{CV\_max}}] \end{aligned} \tag{10}$$

The rectifier used in this IPT system is composed of diodes, and the $P_{\mathrm{Rectifier}}$ is mainly the conduction loss of the diode,

which can be calculated as [38]

$$P_{\mathrm{Rectifier}} = \frac{4\sqrt{2}}{\pi} V_{\mathrm{RF}} I_{\mathrm{S}} + 2 r_{\mathrm{RD}} I_{\mathrm{S}}^2 \tag{11}$$

where V_{RF} is the diode forward voltage and r_{RD} is the equivalent on-state resistance of the diodes in the rectifier. Since the system achieves constant outputs, it can be assumed that the I_{S} remains constant when the coupling coefficient and load are varied. Therefore, the rectifier loss does not need to be considered

$$\begin{aligned} & f_{\mathrm{loss}}\left(Z_{\mathrm{P}}, Z_{\mathrm{S1}}, Z_{\mathrm{S2}}, Z_{\mathrm{S3}}, Z_{\mathrm{T1}}, Z_{\mathrm{T2}}, E\right) \\ & = \int_{M_{\min}}^{M_{\max}} \int_{R_{\mathrm{CC\_min}}}^{R_{\mathrm{CC\_max}}} P_{\mathrm{Coils}}(M, R_1) \\ & \quad + P_{\mathrm{Inverter}}(M, R_1) dR_1 dM \\ & + \int_{M_{\min}}^{M_{\max}} \int_{R_{\mathrm{CV\_min}}}^{R_{\mathrm{CV\_max}}} P_{\mathrm{Coils}}(M, R_2) \\ & \quad + P_{\mathrm{Inverter}}(M, R_2) dR_2 dM \\ & \text{s.t.} \angle Z_{\mathrm{in}}(M, R_1) > 0, \angle Z_{\mathrm{in}}(M, R_2) > 0, M \in [M_{\min}, M_{\max}] \\ & R_1 \in [R_{\mathrm{CC\_min}}, R_{\mathrm{CC\_max}}], R_2 \in [R_{\mathrm{CV\_min}}, R_{\mathrm{CV\_max}}] \end{aligned} \tag{12}$$

The optimization objective of the system's total power losses can be defined as the integral of the power losses over the operating range of the IPT system, as shown in (12)

$$\begin{cases} \mathrm{Min}\left[\mathrm{f_I}\left(\mathrm{Z_P}, \mathrm{Z_{S1}}, \mathrm{Z_{S2}}, \mathrm{Z_{S3}}, \mathrm{Z_T}, \mathrm{E}\right)\right] \\ \mathrm{Min}\left[\mathrm{f_U}\left(\mathrm{Z_P}, \mathrm{Z_{S1}}, \mathrm{Z_{S2}}, \mathrm{Z_{S3}}, \mathrm{Z_T}, \mathrm{E}\right)\right] \\ \mathrm{Min}\left[\mathrm{f_{loss}}\left(\mathrm{Z_P}, \mathrm{Z_{S1}}, \mathrm{Z_{S2}}, \mathrm{Z_{S3}}, \mathrm{Z_T}, \mathrm{E}\right)\right] \\ \mathrm{s.t.} \angle Z_{\mathrm{in}}(M, R_1) > 0, \angle Z_{\mathrm{in}}(M, R_2) > 0, \\ M \in [M_{\min}, M_{\max}]\, R_1 \in [R_{\mathrm{CC\_min}}, R_{\mathrm{CC\_max}}], \\ R_2 \in [R_{\mathrm{CV\_min}}, R_{\mathrm{CV\_max}}] \end{cases} \tag{13}$$

In summary, the system optimization objective functions are modeled as (13).

D. Design Process

First, the operating frequency f, rated output current I_{N}, rated output voltage E, and the range of equivalent loads $[R_{\mathrm{CC\_min}}, R_{\mathrm{CC\_max}}]$, $[R_{\mathrm{CV\_min}}, R_{\mathrm{CV\_max}}]$ in CC and CV modes of the IPT system are determined according to the charging requirements. Then, the range of the mutual inductance $[M_{\min}, M_{\max}]$ is determined. Next, the total number of iterations of the NSGA-II algorithm T and the total number of particles N are determined. Since the compensation topology design of the IPT system does not limit the computational speed of the algorithm, the number of iterations T and the total number of particles N can be appropriately taken to be larger for the sake of the computational accuracy and searching capability. The subspace ranges of the design variables Z_{P}, Z_{S1}, Z_{S2}, Z_{S3}, Z_{T1}, Z_{T2}, and E can be obtained through (4) and (5). Finally, the optimal solution is obtained according to the parameter design flowchart shown in Fig. 5.

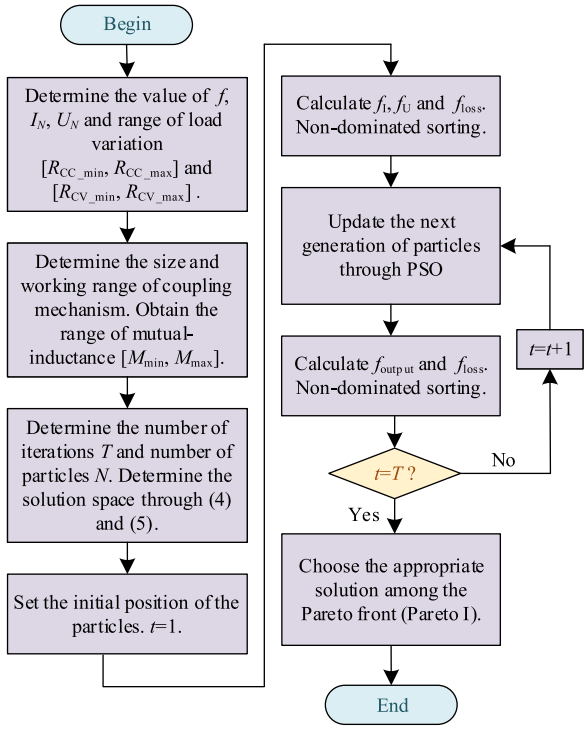

Fig. 5. Design algorithm based on NSGA-II.

TABLE I
PREDETERMINED PARAMETERS OF THE SYSTEM

Parameters	Value
Frequency f	85 kHz
Output current I_{N}	4 A
Output voltage U_{N}	96 V
Transmitting coil self-inductance L_{P}	143 μH
Receiving coil self-inductance L_{S}	135 μH
Load resistance with CC mode R_{CC}	[21 Ω, 24 Ω]
Load resistance with CV mode R_{CV}	[24 Ω, 240 Ω]
Mutual-inductance M	[20 μH, 30 μH]

E. Design Example

The predetermined parameters of the IPT system are shown in Table I, where the variations of the load and mutual inductance are given. Based on these parameters and the flowchart in Fig. 5, the Pareto Front of the compensation topology design of the IPT system with different variable components is calculated by MATLAB, which corresponds to the three cases in Fig. 3(a)–(c), respectively. The number of iterations T is 1000. the total number of particles N is 500. The appropriate scheme is selected from the Pareto Front considering the system power losses and the output fluctuation demands in CC-CV charging, i.e., the objective function (13).

In Fig. 6, three cases are put in the same graph to visualize and compare. It can be seen that when both f_{I} and f_{U} are small, the f_{loss} will be large; when the f_{loss} is small, f_{I}, and f_{U} are large.

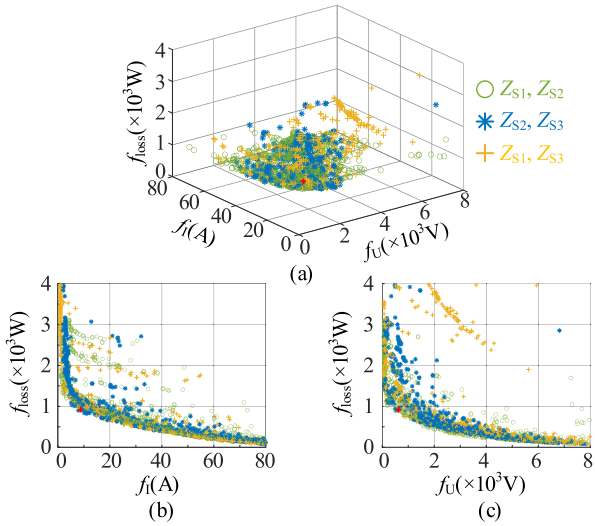

Fig. 6. Pareto Front for the compensation topology: (a) f_{loss} versus f_{I} and f_{U}, (b) with f_{I}, and (c) with f_{U}.

TABLE II
CALCULATED PARAMETERS OF THE SYSTEM

parameters	Designed Value	parameters	Designed Value
Z_{p}/nF	28.66	Z_{S2}/nF	77.81
Z_{S1}/nF, Z_{T1}/nF	50.78, 28	Z_{S3}/μH, Z_{T2}/μH	81.18, 10.66

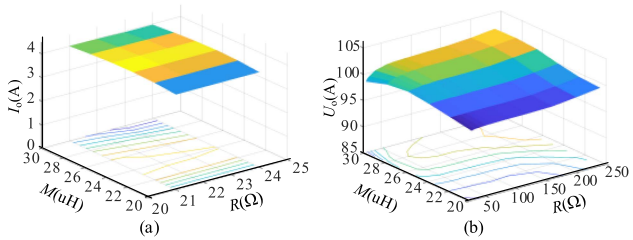

Fig. 7. Simulated output current I_{O} and voltage U_{O} varying with the load R and mutual inductance M. (a) I_{O} in CC mode. (b) U_{O} in CV mode.

To achieve the case shown in the objective function (13), it is needed to have f_{I}, f_{U}, and f_{loss} as low as possible. The three cases are compared and when Z_{s1} and Z_{s3} are chosen as the switching elements, the system produces smaller total losses at smaller current and voltage fluctuations. Therefore, it is considered that the case of Z_{s1} and Z_{s3} chosen as the switching elements is the best.

The appropriate solution can be selected in the Pareto Front according to the total power losses and fluctuation requirements. All the results obtained from the algorithm are prioritized in Pareto Front. For the experimental verification, a typical set of parameters is selected, as shown in Table II.

The simulation results using the optimal parameters are shown in Fig. 7. In CC mode, the output current fluctuates by a maximum of 0.55% when the mutual inductance varies from 20 μH to 30 μH and the load varies from 21 Ω to 24 Ω. As shown

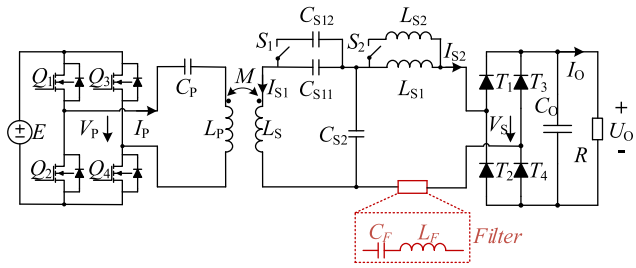

Fig. 8. Optimal topology with *LC* filter.

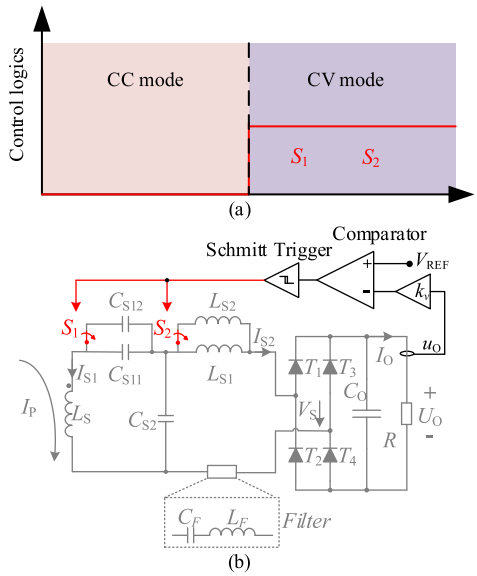

Fig. 9. (a) Control logic for S_1 and S_2 of the IPT system. (b) Control diagram for the IPT system.

in Fig. 7(b), the maximum fluctuation of the voltage is 1.52% versus mutual inductance changing from 20 μH to 30 μH and load varying from 24 Ω to 240 Ω. It can be seen that the charging current in CC mode and charging voltage in CV mode can be regarded as relatively constant.

IV. EXPERIMENTAL VALIDATION

The topology after optimization is shown in Fig. 8 according to the selected parameters. In Fig. 8, C_{P} is the primary-side compensation capacitor. L_{P} and L_{S} are the self-inductances of the primary and secondary coils, respectively. M is the mutual inductance. C_{S11}, C_{S2}, and L_{S1} (C_{S12}, C_{S2}, and L_{S2}) form the LCC compensation network on the secondary side. After the full-bridge rectifier (T_1–T_4) and filter capacitor C_{O}, U_{O}, and I_{O} are used to charge the battery, denoted as the varying load R. In addition, a series resonant filter consisting of capacitor C_{F} and inductor L_{F} is added to attenuate harmonics if necessary [39]. Moreover, C_{F} and L_{F} should satisfy the resonance relationship.

The control logic for switches S_1 and S_2 to achieve CC and CV are shown in Fig. 9. $k_v = V_{\text{REF}}/U_{\text{O}}$ is the voltage ratio. u_{O} is the charging voltage of the IPT system, which is obtained by sampling. $U_{\text{O-S}}$ is the critical voltage of switching. When the

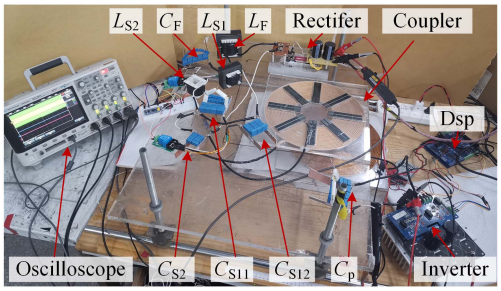

Fig. 10. Experimental prototype.

TABLE III
EXPERIMENTAL PARAMETERS VALUE OF THE SYSTEM

parameters	Value	parameters	Value
C_P/nF	28.5	L_{S1}/μH, L_{S2}/μH	12.96, 82.4
C_{S11}/nF, C_{S12}/nF	30.11, 22.8	C_F/nF	28.05
C_{S2}/nF	77.3	L_F/μH	125

output mode is 4 A/96 V, $U_{O\text{-}S}$ is set to 96 V. During the CC charging process, u_O gradually increases. When $u_O \geq U_{O\text{-}S}$, the controller will transmit a switching signal to the switches. The switches S_1 and S_2 are toggled and the system is operating in CV mode. In CV mode, the charging voltage is maintained at U_O, and the charging current I_O starts to decrease until it hits the end-of-charge current. In general, when S_1 and S_2 are ON, the system operates in CC mode. On the other hand, when S_1 and S_2 are OFF, the system operates in CV mode.

To demonstrate the applicability of validating the proposed topology and the above analysis, an experimental prototype is constructed and displayed in Fig. 10. A set of parameters was determined for the topology and subsequently measured. Since the misalignment tolerance of the compensation topology designed by the NSGA-II is not limited by the loosely coupled transformer, a commonly used circular pad is adopted. The designed parameters are listed in Table III. The four MOSFETs (Q_1–Q_4) use C2M0040120D, while the four rectifier diodes (T_1–T_4) use GP2D050A120B. Litz wire and the ferrite core specifications are AWG38 × 3.9 mm and PC40, respectively. The input voltage is given by the dc power source Chroma 62150H-600. The oscilloscope Agilent DSO-X3034A is used to verify the performance of the system. The battery load R is replaced by an electronic load IT8816B. The experimental prototype uses an open-loop controller for the primary inverter to demonstrate that the proposed method allows the system to resist coupling coefficient and load variations.

A. Results of CC and CV Outputs

In CC mode, the output current fluctuation range ΔI_O is defined by (14), where $I_{O\max}$ and $I_{O\min}$ are the maximum and minimum output currents of the IPT system with varying R. Likewise, in CV mode, the output voltage fluctuation range ΔU_O is defined by (15), where $U_{O\max}$ and $U_{O\min}$ are the

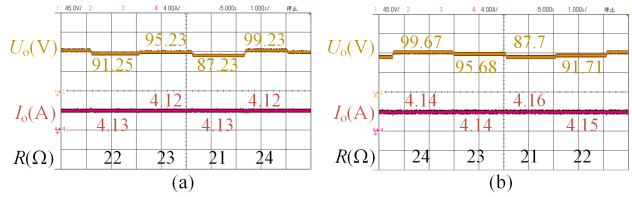

Fig. 11. Experimental waveforms of U_O and I_O when R changes from 21 Ω to 24 Ω with different M in CC mode. (a) $M = 20$ μH. (b) $M = 28$ μH.

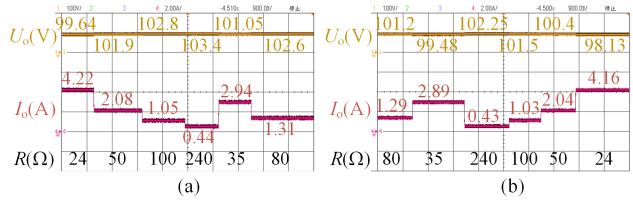

Fig. 12. Experimental waveforms of U_O and I_O when R changes from 24 Ω to 240 Ω with different M in CV mode. (a) $M = 24$ μH. (b) $M = 30$ μH.

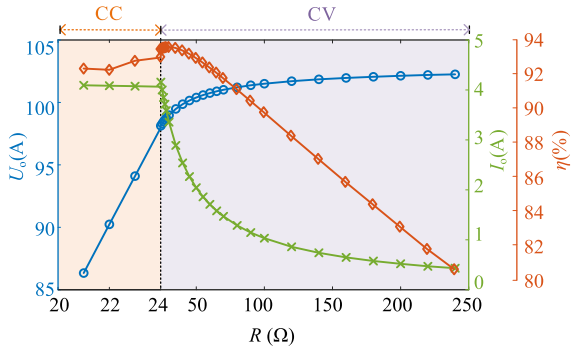

Fig. 13. Charging curves measured at maximum M.

maximum and minimum output voltages of the IPT system [29]

$$\Delta I_O = \frac{I_{O\max} - I_{O\min}}{I_{O\max} + I_{O\min}} \tag{14}$$

$$\Delta U_O = \frac{U_{O\max} - U_{O\min}}{U_{O\max} + U_{O\min}} \tag{15}$$

In CC mode, Fig. 11(a) shows the waveforms of I_O when $M = 20$ μH and R varies from 21 Ω to 24 Ω. The current fluctuation range of I_O is 0.12%. Fig. 11(b) shows the output waveforms when $M = 28$ uH and R varies from 21 Ω to 24 Ω. The current fluctuation range of I_O is only 0.24%. The system has a strong ability to achieve constant current output.

In CV mode, Fig. 12(a) shows the waveforms of U_O when $M = 24$ μH and R varies from 24 Ω to 240 Ω. The voltage fluctuation range of U_O is 1.85%. Fig. 12(b) shows the output waveforms when $M = 30$ μH and R varies from 24 Ω to 240 Ω. The voltage fluctuation range of U_O is 2.05%. The system also shows a strong ability to achieve constant voltage output.

The output voltage U_O, output current I_O, and efficiency η of the system at $M = 30$ μH are shown in Fig. 13. The ΔI_O in CC mode and ΔU_O in CV mode are calculated as 0.34% and 2.05%, respectively. Though there is tolerance between the parameters

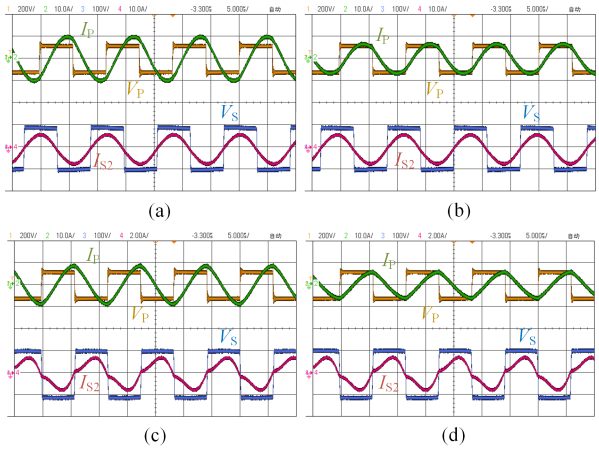

Fig. 14. Experimental waveforms of I_P, V_P, V_S, and I_{S2} with maximum and minimum M.

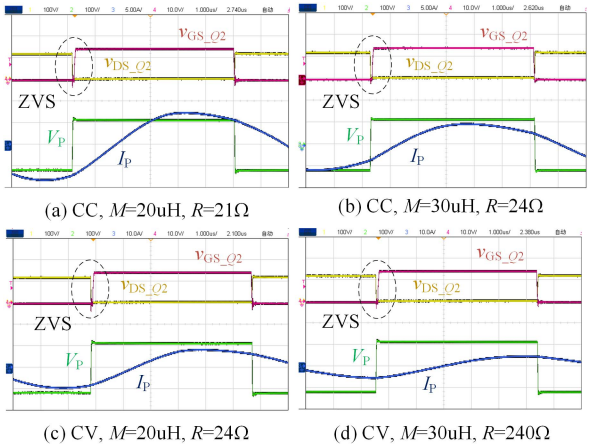

Fig. 15. Experimental waveforms of I_P, V_P, and Q_2 with maximum and minimum M.

used in the experiment and those obtained from the algorithm, the current and voltage fluctuations are both less than 5%, which means the IPT system performs well in CC and CV modes. The system efficiency reaches a maximum value of 93.5% at $R = 30\ \Omega$. Besides, the output power decreases as R increases, with a minimum efficiency of 81.02% when R is 240 Ω.

B. Results of Misalignment Tolerance

When M is the maximum ($M = 30\ \mu$H) or the minimum ($M = 20\ \mu$H) value, the waveforms of the output voltage V_P and output current I_P of the system inverter and the input voltage V_S and input current I_{S2} of the secondary full-bridge rectifier are shown in Fig. 14. It is obvious that the input impedance of the system is inductive both in CC mode and CV mode, which is coincident with the objective function (8).

To demonstrate that the ZVS condition is achieved, the experimental waveforms of drain-source voltage v_{DS_Q2} and gate-source voltage v_{GS_Q2} of Q_2 are shown in Fig. 15. The voltage is measured considering the variation of the mutual inductance

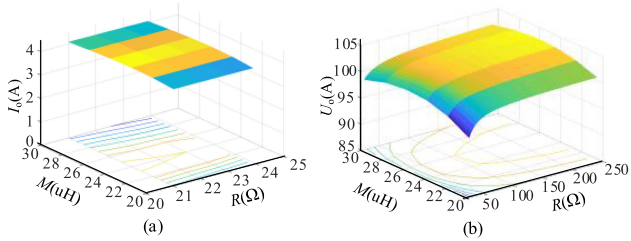

Fig. 16. Measured output current I_O and voltage U_O varying with the load R and mutual inductance M. (a) I_O in CC mode. (b) U_O in CV mode.

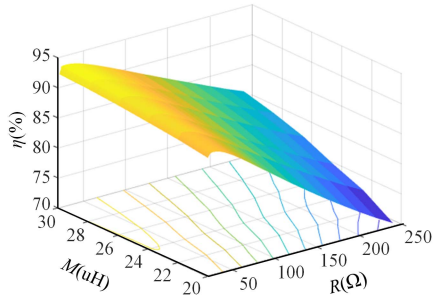

Fig. 17. Measured efficiency η varying with load R and mutual inductance M.

and load. It shows that before the v_{GS_Q2} rise, the v_{DS_Q2} had already fallen to zero, which indicates that the ZVS turn-ON for the MOSFETs is achieved. The phase angle between I_P and V_P might be large under some special conditions [see Fig. 15(d)], but the total losses of the system are the lowest. This is because the total lower losses of the whole charging conditions (CC-CV charging with the ranges of equivalent load varying from 21 Ω to 240 Ω and the mutual inductance varying from 20 μH to 30 μH, respectively) is one of the optimal objectives, making the system more efficient under all the conditions.

The output current I_O of the system in CC mode is shown in Fig. 16(a). It is indicated that the output current fluctuates by a maximum of 0.34% when the mutual inductance varies from 20 μH to 30 μH and the load varies from 21 Ω to 24 Ω.

It can be indicated from Fig. 16(b) that the system can tolerate the mutual inductance changing from 20 μH to 30 μH within the load varying from 24 Ω to 240 Ω, and the output voltage fluctuates by a maximum of 2.69% in CV mode. It is considered that the parameters calculated by the algorithm can realize CV within the constraints. Generally, the fluctuations of voltage and current both less than 5% enable the system to realize CC-CV charging well. The feasibility of the NSGA-II algorithm applied to the parameter design of IPT systems is verified. Compared with the simulation results shown in Fig. 7, the current in CC mode and the voltage in CV mode are 2.34% and 2.3% higher than that in the simulation, respectively. It is reasonable that there is a tolerance between the experimental and simulation parameters.

The measured efficiency is from the dc power source to the dc output. The efficiency of the system η is shown in Fig. 17, where the maximum efficiency is 93.5% at $M = 30\ \mu$H and the minimum efficiency is 70.5% at $M = 20\ \mu$H.

TABLE IV
COMPARISON WITH OTHER METHODS ACHIEVED CC-CV REPORTED IN THE LITERATURE

Ref.	Component number (coil +compensation component +switch +rectifier)	Load variation		Misalignment tolerance		Fluctuation	
		R_{CC}/Ω	R_{CV}/Ω	k	M/uH	CC	CV
[30]	4+5+0+2	25-43	55-300	0.1-0.2	/	5%	5%
[31]	4+11+1+1	36-42	42-410	0.1-0.2	/	4.2%	4.2%
[32]	4+12+2+1	36-48	48-480	/	25-40	5%	5%
[33]	4+11+2+1	15-18	19-70	/	18–34	5%	5%
This work	2+6+2+1	21-24	24-240	0.15-0.22	20-30	0.34%	2.69%

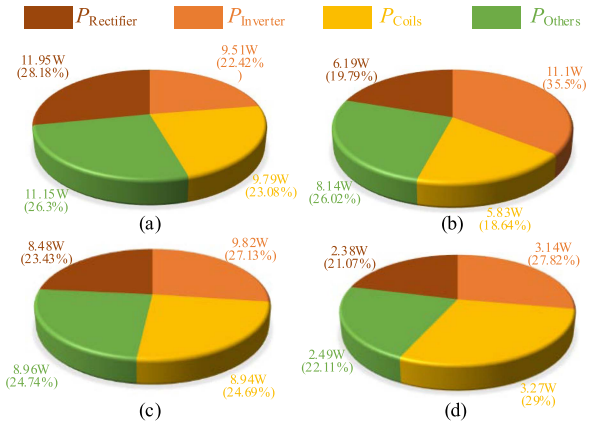

Fig. 18. Power losses of the proposed IPT system. (a) In CC mode, $R = 21\ \Omega$, $M = 20\ \mu$H. (b) In CC mode, $R = 23\ \Omega$, $M = 30\ \mu$H. (c) In CV mode, $R = 24\ \Omega$, $M = 26\ \mu$H. (d) In CV mode, $R = 240\ \Omega$, $M = 28\ \mu$H.

C. Analysis of Power Loss

To further illustrate the distribution of power losses, the power losses of the proposed IPT system are given in Fig. 18. The conduction loss on the passive components and the conduction loss of the wires are relatively difficult to measure, so these types of power losses are categorized as P_{Others}.

D. Discussion

To show the advantages of the proposed method, the performance of the proposed approach is compared with other methods, as presented in Table IV.

Compared with other methods in [30], [31], [32], and [33], the number of all the components of the proposed method is the fewest. Besides, the variations of the load and the coupling coefficient or the mutual inductance are acceptable and comparable. Moreover, this work's current fluctuation in CC mode and the voltage fluctuation in CV mode are the lowest. Therefore, the proposed method for CC-CV charging against varying mutual inductance and load is significantly superior to the other methods.

For this IPT system, with seven variables, three objectives, and a few limitations, selecting the parameters takes a large calculation. Therefore, the NSGA-II algorithm [35], which has outstanding advantages (easy to implement, fast convergence speed with high accuracy) is specifically chosen to select the parameters. Moreover, it can use other algorithms to obtain the parameters if there are any better ones calculating faster and more accurately.

V. CONCLUSION

A method for optimizing the compensation parameters of the IPT system is proposed in this article. It is designed to realize CC and CV outputs with misalignment tolerance for battery charging. The NSGA-II algorithm is used to design the compensation components of the system. The compensation components are not predefined as inductors or capacitors, they are decided by the appropriate parameters after the optimization according to the requirements. An experimental prototype is built to verify the proposed method. The results show that when the load varies from 21 Ω to 240 Ω and the mutual inductance varies from 20 μH to 30 μH, the system can achieve CC-CV charging. The fluctuation of current in CC mode is less than 0.34%, the fluctuation of voltage in CV mode is less than 2.69%, and the maximum efficiency reaches 93.5%, which shows a great performance of the proposed method for the IPT system considering the mutual inductance and load variations. In the future, the optimization including the ESRs of the coupling coils will be considered.

REFERENCES

[1] X. Yi, W. Zheng, H. Cao, S. Wang, X. Feng, and Z. Yang, "Wireless power transmission for implantable medical devices using focused ultrasound and a miniaturized 1-3 piezoelectric composite receiving transducer," *IEEE Trans. Ultrasonics, Ferroelect., Freq. Control*, vol. 68, no. 12, pp. 3592–3598, Dec. 2021.

[2] C. Cai, J. Wang, M. Saeedifard, P. Zhang, R. Chen, and J. Zhang, "Gyrator-gain variable WPT topology for MC-unconstrained CC output customization using simplified capacitance tuning," *IEEE Trans. Ind. Electron.*, vol. 71, no. 4, pp. 3594–3605, Apr. 2024.

[3] Z. Zhang et al., "A dynamic wireless power transfer system using DC controlled variable inductor for segment transmitter automatic switching," *IEEE Trans. Power Electron.*, to be published, doi: 10.1109/TPEL.2024.3426100.

[4] X. Liu, F. Gao, H. Niu, G. Sun, T. Wang, and H. Wang, "A series–Parallel transformer-based WPT system for 400-V and 800-V electric vehicles with Z1 or Z2 class," *IEEE Trans. Power Electron.*, vol. 39, no. 1, pp. 1749–1761, Jan. 2024.

[5] J. Wang, C. Wang, Z. Lu, Z. Guo, and S. Wang, "Single-switch wireless-power-transfer circuit with P-CLC compensation network used for battery charging," *IEEE Trans. Transp. Electrific.*, vol. 8, no. 3, pp. 4014–4026, Sep. 2022.

[6] X. Qu, H. Chu, S.-C. Wong, and C. K. Tse, "An IPT battery charger with near unity power factor and load-independent constant output combating design constraints of input voltage and transformer parameters," *IEEE Trans. Power Electron.*, vol. 34, no. 8, pp. 7719–7727, Aug. 2019.

[7] Z. Zhang, F. Zhu, D. Xu, P. T. Krein, and H. Ma, "An integrated inductive power transfer system design with a variable inductor for misalignment tolerance and battery charging applications," *IEEE Trans. Power Electron.*, vol. 35, no. 11, pp. 11544–11556, Nov. 2020.

[8] K. Song et al., "A control strategy for wireless EV charging system to improve weak coupling output based on variable inductor and capacitor," *IEEE Trans. Power Electron.*, vol. 37, no. 10, pp. 12853–12864, Oct. 2022.

[9] M. Kim, D.-M. Joo, and B. K. Lee, "Design and control of inductive power transfer system for electric vehicles considering wide variation of output voltage and coupling coefficient," *IEEE Trans. Power Electron.*, vol. 34, no. 2, pp. 1197–1208, Feb. 2019.

[10] L. Zhao, D. J. Thrimawithana, U. K. Madawala, A. P. Hu, and C. C. Mi, "A misalignment-tolerant series-hybrid wireless EV charging system with integrated magnetics," *IEEE Trans. Power Electron.*, vol. 34, no. 2, pp. 1276–1285, Feb. 2019.

[11] H. Feng, T. Cai, S. Duan, X. Zhang, H. Hu, and J. Niu, "A dual-side-detuned series–Series compensated resonant converter for wide charging region in a wireless power transfer system," *IEEE Trans. Ind. Electron.*, vol. 65, no. 3, pp. 2177–2188, Mar. 2018.

[12] X. Qu, Y. Jing, H. Han, S.-C. Wong, and C. K. Tse, "Higher order compensation for inductive-power-transfer converters with constant-voltage or constant-current output combating transformer parameter constraints," *IEEE Trans. Power Electron.*, vol. 32, no. 1, pp. 394–405, Jan. 2017.

[13] Y. Wang et al., "A double-T-type compensation network and its tuning method for IPT system," *IEEE Trans. Ind. Appl.*, vol. 53, no. 5, pp. 4757–4767, Sep./Oct. 2017.

[14] X. Mao, J. Chen, Y. Zhang, and J. Dong, "A simple and reconfigurable wireless power transfer system with constant voltage and constant current charging," *IEEE Trans. Power Electron.*, vol. 37, no. 5, pp. 4921–4925, May 2022.

[15] D. Wang, X. Qu, Y. Yao, and P. Yang, "Hybrid inductive-power-transfer battery chargers for electric vehicle onboard charging with configurable charging profile," *IEEE Trans. Intell. Transp. Syst.*, vol. 22, no. 1, pp. 592–599, Jan. 2021.

[16] Z. Huang, G. Wang, J. Yu, and X. Qu, "A novel clamp coil assisted IPT battery charger with inherent CC-to-CV transition capability," *IEEE Trans. Power Electron.*, vol. 36, no. 8, pp. 8607–8611, Aug. 2021.

[17] Y. Chen et al., "A clamp circuit-based inductive power transfer system with reconfigurable rectifier tolerating extensive coupling variations," *IEEE Trans. Power Electron.*, vol. 39, no. 2, pp. 1942–1946, Feb. 2024.

[18] C. Ma, R. Yao, C. Li, and X. Qu, "A Family of IPT battery chargers with small clamp coil for configurable and self-sustained battery charging profile," *IEEE Trans. Power Electron.*, vol. 38, no. 6, pp. 7910–7919, Jun. 2023.

[19] J. Mai, Y. Wang, Y. Yao, M. Sun, and D. Xu, "High-misalignment-tolerant IPT systems with solenoid and double D pads," *IEEE Trans. Ind. Electron.*, vol. 69, no. 4, pp. 3527–3535, Apr. 2022.

[20] A. Zaheer, G. A. Covic, and D. Kacprzak, "A bipolar pad in a 10-kHz 300-W distributed IPT system for AGV applications," *IEEE Trans. Ind. Electron.*, vol. 61, no. 7, pp. 3288–3301, Jul. 2014.

[21] S. Y. Choi, J. Huh, W. Y. Lee, and C. T. Rim, "Asymmetric coil sets for wireless stationary EV chargers with large lateral tolerance by dominant field analysis," *IEEE Trans. Power Electron.*, vol. 29, no. 12, pp. 6406–6420, Dec. 2014.

[22] Y. Zhang, S. Chen, X. Li, and Y. Tang, "Design methodology of free-positioning nonoverlapping wireless charging for consumer electronics based on antiparallel windings," *IEEE Trans. Ind. Electron.*, vol. 69, no. 1, pp. 825–834, Jan. 2022.

[23] P. Zhang, M. Saeedifard, O. C. Onar, Q. Yang, and C. Cai, "A field enhancement integration design featuring misalignment tolerance for wireless EV charging using LCL topology," *IEEE Trans. Power Electron.*, vol. 36, no. 4, pp. 3852–3867, Apr. 2021.

[24] Y. Chen et al., "A hybrid inductive power transfer system with misalignment tolerance using quadruple-D quadrature pads," *IEEE Trans. Power Electron.*, vol. 35, no. 6, pp. 6039–6049, Jun. 2020.

[25] L. Zhao, D. J. Thrimawithana, and U. K. Madawala, "Hybrid bidirectional wireless EV charging system tolerant to pad misalignment," *IEEE Trans. Ind. Electron.*, vol. 64, no. 9, pp. 7079–7086, Sep. 2017.

[26] X. Qu, Y. Yao, D. Wang, S.-C. Wong, and C. K. Tse, "A Family of hybrid IPT topologies with near load-independent output and high tolerance to pad misalignment," *IEEE Trans. Power Electron.*, vol. 35, no. 7, pp. 6867–6877, Jul. 2020.

[27] H. Feng, T. Cai, S. Duan, J. Zhao, X. Zhang, and C. Chen, "An LCC-compensated resonant converter optimized for robust reaction to large coupling variation in dynamic wireless power transfer," *IEEE Trans. Ind. Electron.*, vol. 63, no. 10, pp. 6591–6601, Oct. 2016.

[28] J. Mai, Y. Wang, Y. Yao, and D. Xu, "Analysis and design of high-misalignment-tolerant compensation topologies with constant-current or constant-voltage output for IPT systems," *IEEE Trans. Power Electron.*, vol. 36, no. 3, pp. 2685–2695, Mar. 2021.

[29] Y. Yao, Y. Wang, X. Liu, Y. Pei, D. Xu, and X. Liu, "Particle swarm optimization-based parameter design method for S/CLC-compensated IPT systems featuring high tolerance to misalignment and load variation," *IEEE Trans. Power Electron.*, vol. 34, no. 6, pp. 5268–5282, Jun. 2019.

[30] G. Li and H. Ma, "A hybrid IPT system with high-misalignment tolerance and inherent CC–CV output characteristics for EVs charging applications," *IEEE J. Emerg. Sel. Topics Power Electron.*, vol. 10, no. 3, pp. 3152–3160, Jun. 2022.

[31] Y. Wang, H. Liu, F. Wu, P. Wheeler, Q. Zhou, and S. Zhao, "Research on a three-coil hybrid IPT charger with improved tolerance to coupling variation and load-independent output," *IEEE J. Emerg. Sel. Topics Ind. Electron.*, vol. 4, no. 2, pp. 625–636, Apr. 2023.

[32] L. Ji, M. Zhang, B. Qian, and H. Sun, "A series of hybrid WPT systems with automatic switching between constant-current and constant-voltage modes on the secondary side," *IEEE J. Emerg. Sel. Topics Power Electron.*, vol. 11, no. 1, pp. 361–371, Feb. 2023.

[33] Y. Chen, B. Yang, Z. Kou, Z. He, G. Cao, and R. Mai, "Hybrid and reconfigurable IPT systems with high-misalignment tolerance for constant-current and constant-voltage battery charging," *IEEE Trans. Power Electron.*, vol. 33, no. 10, pp. 8259–8269, Oct. 2018.

[34] Z. Gong, J. Li, and X. Tong, "Misalignment-tolerant series hybrid with active adjustable constant current and constant voltage output wireless charging system," *Energies*, vol. 14, no. 22, p. 7594, Nov. 2021, doi: 10.3390/en14227594.

[35] K. Deb, A. Pratap, S. Agarwal, and T. Meyarivan, "A fast and elitist multiobjective genetic algorithm: NSGA-II," *IEEE Trans. Evol. Computation*, vol. 6, no. 2, pp. 182–197, Apr. 2002.

[36] W. Tang, L. Jing, W. Cao, W. Xu, X. Wu, and H. Liao, "Optimization of magnetic coupling mechanism of dynamic wireless power transfer based on NSGA-II algorithm," *Sci. Rep.*, vol. 14, no. 1, 2024, Art. no. 5121.

[37] Y. Li et al., "Extension of ZVS region of series–Series WPT systems by an auxiliary variable inductor for improving efficiency," *IEEE Trans. Power Electron.*, vol. 36, no. 7, pp. 7513–7525, Jul. 2021.

[38] J. Cai et al., "Zero-voltage switching regulation strategy of full-bridge inverter of inductive power transfer system decoupled from output characteristics," *IEEE Trans. Power Electron.*, vol. 37, no. 11, pp. 13861–13873, Nov. 2022.

[39] B. Yang et al., "A design method to minimize detuning for double-sided LCC-compensated IPT system improving efficiency versus air gap variation," *IEEE Trans. Power Electron.*, vol. 39, no. 1, pp. 1723–1737, Jan. 2024.

Qi Wang received the B.Sc. degree in transport equipment and control engineering electrical in 2022 from the School of Mechanical Engineering, Southwest Jiaotong University, Chengdu, China, where she is currently working toward the M.Sc. degree in electrical engineering with the School of Electrical Engineering.

Her main research interest includes wireless power transfer.

Zheng Li received the B.Sc. degree in electrical engineering and automation from the School of Electrical and Automation Engineering, East China Jiaotong University, Nanchang, China, in 2022. He is currently working toward the M.Sc. degree in electrical engineering with the School of Electrical Engineering, Southwest Jiaotong University, Chengdu, China.

His main research interest includes wireless power transfer.

Bin Yang (Member, IEEE) received the Ph.D. and B.S. degrees in electrical engineering at the School of Electrical Engineering, Southwest Jiao tong University, Chengdu, China and electrical engineering at the School of Electrical and Automation Engineering, East China Jiaotong University, Nanchang, China, in 2024 and 2017, respectively.

From 2023 to 2024, he was a Visiting Scholar founded by the China Scholarship Council with the Department of Energy, Aalborg University, Aalborg, DK. He is currently intermediate engineer with China Electronics Technology Group Corporation Tenth Research Institute. His research focuses on wireless power transfer, Antenna design and beamforming.

Yuanfang Lu received the B.S. and M.S. degrees in electrical engineering from Southwest Jiaotong University, Chengdu, China, in 2019 and 2022, respectively. He is currently working toward the Ph.D. degree in electrical engineering with the State Key Laboratory of Alternate Electrical Power System with Renewable Energy Sources, North China Electric Power University, Beijing, China.

His research interests include condition monitoring of power electronic device and wireless power transfer.

Ruikun Mai (Senior Member, IEEE) received the B.Sc. and Ph.D. degrees in electrical engineering from the School of Electrical Engineering, Southwest Jiaotong University, Chengdu, China, in 2004 and 2010, respectively.

He is currently a Professor with the School of Electrical Engineering, Southwest Jiaotong University, Chengdu, China. His research interests include wireless power transfer and its application in railway systems, power system stability, and control.

Zhengyou He (Senior Member, IEEE) received the B.Sc. and M.Sc. degrees in computational mechanics from Chongqing University, Chongqing, China, in 1992 and 1995, respectively, and the Ph.D. degree in electrical engineering from the School of Electrical Engineering, Southwest Jiaotong University, Chengdu, China, in 2001.

He is currently a Professor with the School of Electrical Engineering, Southwest Jiaotong University. His research interests include signal process and information theory applied to electrical power system, and application of wavelet transforms in power system.

Yang Chen (Senior Member, IEEE) received the B.Sc. degree in electrical engineering and automation and the Ph.D. degree in electrical engineering from Southwest Jiaotong University, Chengdu, China, in 2015 and 2020, respectively.

From 2018 to 2019, he was a Visiting Scholar founded by the China Scholarship Council with the Future Energy Electronics Center, Virginia Tech, Blacksburg, VA, USA. From 2020 to 2023, he was a Postdoctoral Researcher with Southwest Jiaotong University, Chengdu, China, where he is currently an Associate Researcher. His research interest includes wireless power transfer.

Dr. Chen was the recipient of the 2023 Outstanding Reviewer Award from IEEE TRANSACTIONS ON POWER ELECTRONICS.